The Diagnostic Utility of Negative-Staining Electron Microscopy in the Urine for the Detection of Polyoma-BK-virus Infections : A Comparative Analysis of Electron Microscopy, Conventional Cytology, and Quantitative PCR.

Singh HK, Shen YJ, Madden V, Thompson D, and Nickeleit V
Department of Pathology and Laboratory Medicine
The University of North Carolina at Chapel Hill
Chapel Hill, North Carolina USA

Polyomavirus allograft nephropathy, also termed BK-virus nephropathy (BKN) after the main causative agent, the polyoma-BK-virus strain (BKV), is a major complication following kidney transplantation. The emergence of BKN since mid-1990 has been well documented. BKN is by far the most important infectious complication affecting kidney transplants with a reported prevalence of 1% to up to 10%. It is most likely caused by the reactivation of latent BK viruses which, under sustained and intensive immunosuppression, enter a replicative/productive cycle. Since effective anti-viral treatment strategies are poorly defined, BKN often leads to severe allograft dysfunction and graft loss. Graft failure rates, especially when BKN is diagnosed late or treatment strategies fail, can reach 50% to 100% within 24 months following the initial diagnosis.

Polyomaviruses of the BK-strain are endemic and often remain latent in the transitional layer of the bladder, ureters, and the renal pelvis, as well as in tubular epithelial cells of the kidney. Slight changes in the immune status/and or an immunocompromised condition can lead to the (re)activation of latent polyomaviruses, especially along the transitional cell layer, leading to the shedding of viral particles in the urine indicated by the detection of inclusion bearing epithelial cells, "decoy cells". These cells can best be identified and quantified in liquid based (Cytyc Inc, Boxborough, MA, and Tripath Imaging Inc., Burlington, NC) Papanicolaou stained urine cytology preparations. The general cut-off values for decoys cells in patients at increased risk for the development of BKN have been the identification of >10 decoys cells/10 high power fields in liquid based cytology spins. A positive screening result (>10 decoys cells/10 high power fields) should be additionally assessed – according to the latest consensus guidelines - with quantitative assays (such as quantitative BKV DNA load measurements in the urine) in order to increase positive predictive values for BKN. The assumption has been made that repeated PCR values above 10^7 BKV copies per milliliter urine are associated with a high risk for BKN.

The current gold standard for establishing a definitive diagnosis of BKN is the renal biopsy. Examination of the biopsy not only allows for histological staging of BKN but, in addition, provides information regarding the presence of concomitant processes such as acute rejection. However, invasive biopsy procedures are not suited as generalized screening tools for assessing the potential risk of BKN.

As indicated above, a number of screening tools have been proposed and tested for the detection of BK virus activation and replication in the urine, including cytology , quantitative BKV DNA (or less commonly RNA) PCR tests. All of these tests have limitations.

Another technique that has previously played a pivotal role in diagnostic virology is negative staining electron microscopy. Negative staining EM of urine specimens can provide a rapid, noninvasive, and relatively inexpensive diagnostic tool for the detection of different virus families that can be distinguished by size. Serial studies can be easily performed and may provide a potentially easy means for monitoring either the persistence or the resolution of viral activation. However, its use for the detection of polyomavirus particles has not been systematically evaluated as a potential rapid screening tool for the identification of patients at high risk for BKN.

There is only one small series from Howell et al evaluating *qualitative* negative staining electron microscopy (EM) for BK polyomavirus particles. EM was performed in 5 patients with biopsy proven BKN and free polyomavirus particles were found in all 5 patients. They also evaluated urine samples by EM in 23 transplant patients with causes of renal dysfunction other than BKN and found no evidence of free virus. Apart from these renal allograft recipients analyzed by Howell, bone marrow transplant recipients have been studied with negative EM staining techniques to search for polyoma viruses in the urine by Biel and colleagues. They evaluated 531 urine samples from 101 patients before and after bone marrow transplantation for the detection of human polyomaviruses by negative staining EM and compared the technique with PCR. The authors reported a linear correlation between the viral load levels detected by PCR and the proportion of free polyoma virus particles seen with negative EM staining. . In the report, however, there was no correlation with urine cytology for decoy cell shedding or with patient outcomes (i.e. asymptomatic viral shedding, development of hemorrhagic cystitis or BKN).

Thus, at present comparative analyses of urine by conventional cytology (i.e., semi-quantitation of decoy cells), quantitative PCR for BKV DNA, and the semi-quantitative EM evaluation for free polyomavirus particles have not been systematically conducted and correlated with the development of viral disease, such as polyoma-BK-virus induced nephropathy. BKN.

Here, we present results from a pilot study of 73 urine samples from 70 patients evaluated by: negative staining EM for free polyomavirus particles, conventional urine cytology (i.e., semi-quantitation of decoy cells), and quantitative PCR for BKV DNA. The diagnostic utility of these techniques will be discussed as it relates to the identification and monitoring of renal transplant patients at risk for the development of BKN.

<u>Materials and Methods:</u>

“Negative staining” refers to the embedding of a specimen in a layer of dried heavy metal solution. Most negative staining protocols involve the adsorption of the specimen to a glow-discharged carbon-coated EM grid, which is washed with deionized water and subsequently stained with a heavy metal solution (uranyl or tungstate stains). Enrichment of virus particles from urine samples can be further accomplished by a series of centrifugation steps before negative staining.

73 urine specimens from 70 patients were prospectively collected, transported at room temperature and stored at 4°C. There were 21 non-transplant and 52 renal transplant patients. 7 of the patients had a biopsy proven diagnosis of BKN and concurrent urine specimens for analysis. All urine samples were processed for conventional urine cytology using standard liquid based cytology protocols (Tripath imaging, Inc, Burlington, NC) and stained by the Papanicolaou method. The supernatant was subsequently centrifuged at 20,000*g* for a short interval to remove large cell debris after which ultracentrifugation at 100,000*g* was performed for viral concentration. The pellet was resuspended in distilled water and negative staining was performed using standard protocols. 1% aqueous uranyl acetate was used for the negative stain. The EM grids were examined on a transmission electron microscope (LEO EM-910, LEO Electron Microscopy, Inc., Thornwood, NY, accelerating voltage 80kV). A thorough search for viral particles was done at high power (>40,000x) and semi-quantitation of viral particles was performed on ten representative 63,000x fields. All EM Grids were examined for an average of 30 minutes by the same electron microscopist. The total time for performance of negative staining EM is approximately 3 hours (includes the time for ultracentrifugation) and total cost (including labor) for this test in our laboratory is $180.00.

Quantitative PCR analysis for BKV DNA was performed using standard protocols (omitting any digestion step) on an aliquot of urine obtained from the supernatant after the cytology specimen preparation.

Results

The ultrastructural morphology of polyomavirus particles after negative staining is shown in Figure 1. The well-characterized regular capsid structure of the viral particles could be readily identified in all positive samples. Viral particles measured approximately 40 – 45 nanometers.

In Table 1, the urine samples were grouped according to decoy cell semi-quantitation (i.e., Group I: no decoy cells; Group II: 1-9 decoy cells/10hpf = no/minimal risk for BKN; Groups III : 10-50 decoy cells/10hpf and Group IV: >50 decoys cells/10hpf = patients at risk for BKN; risk assessment according to previously published reports). The groups were compared with the results from negative staining EM and quantitative PCR. No free virus was detected by negative staining EM below a threshold of 10 decoys cells/10hpf (Group II) whereas BK copies (up to 1.62×10^9 copies /ml) were detected by PCR in some of the samples in group II ("non-diagnostic" background PCR positivity). In groups III and IV (decoy cells 10-50 and >50/10hpf, respectively), the median numbers of free viral particles detected by EM increased as the number of decoy cells increased. No significant increase was noted in group III versus group IV by PCR analysis.

Table 2 summarizes the findings from samples in seven renal transplant patients taken at the time of initial biopsy diagnosis of BKN as compared to the BKN negative renal transplant control group. The median values for decoy cell shedding, free viral particles by EM and quantitative PCR showed differences between the two groups. All patients with BKN demonstrated at least 6 free viral particles/10hpf (median = 62), decoy cell shedding >10/10hpf and a viral load of more than 10^6 BK copies/ml by PCR.

Conclusions of our pilot analysis:

1. Negative staining EM of urine specimens provides a rapid, noninvasive, and relatively inexpensive diagnostic tool for the detection of polyoma viruses in the urine and to identify patients at increased risk for BKN.
2. A presumptive threshold level of ≥6 free viral particles /10hp EM fields was found to identify patients at increased risk for BKN.
3. Negative staining EM to search for free polyomavirus particles has an increased specificity compared to urine PCR tests for identifying patients with BKN.
4. Negative staining EM has the potential additional valuable ability to detect agents other than polyoma viruses, including adenovirus and cytomegalovirus that can also potentially infect the urinary tract of renal transplant patients.
5. From our pilot study, negative staining EM appears to be superior to quantitative urine PCR in assessing the risk for development of BKN.
6. An early diagnosis of BKN is the key for improving renal allograft survival. This can be achieved via aggressive screening programs with the combined use of diagnostic tools that include urine cytology for decoy cells, quantitation of the viral load in urine, and negative staining EM for free polyomavirus particles.

Figure 1: Ultrastructural Features of polyomavirus particles after negative staining.

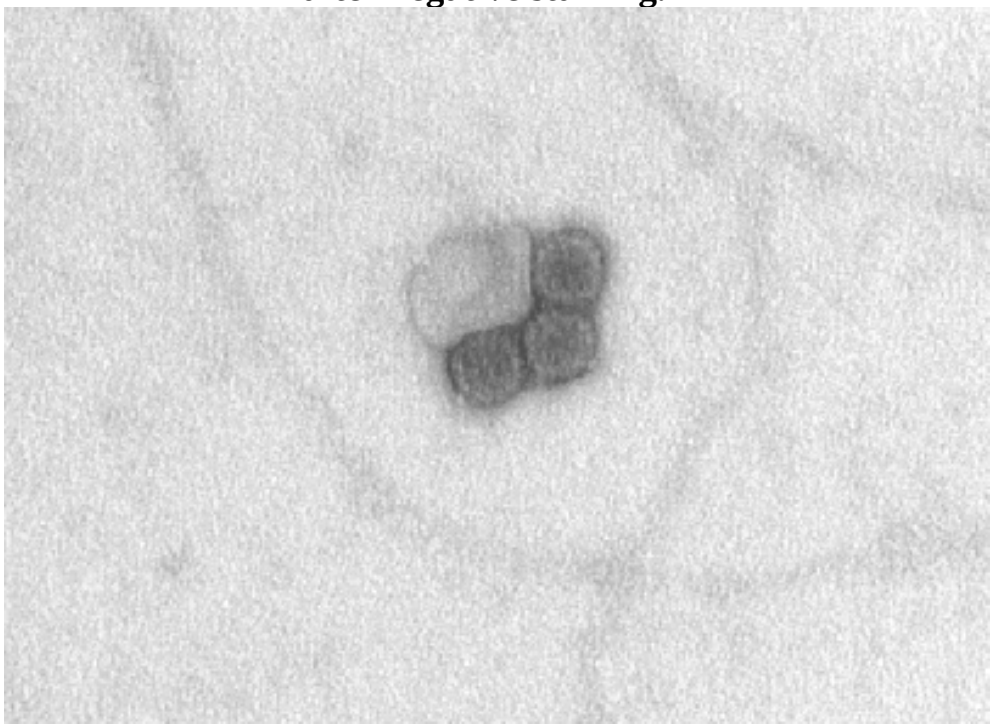

Three polyomavirus particles partially surrounding a fragment of cell membrane are shown after negative staining. Note the regular capsid structure of the polyomavirus particles which measure approximately 40 nanometers each.

Table 1: Comparative Analysis of Conventional Cytology, Negative staining EM, and Quantitative PCR (n = 73 urine samples):

Groups	**Urine Cytology: Decoy Cells*** Median (Range)	**Negative Staining EM**** Median (Range)	**Quantitative Urine PCR***** Median (Range)
Group I: 0 decoy cells (n = 31 samples)	**0 (0)**	**0 (0)**	**0 (0)**
Group II: 1-9 decoy cells (n = 15 samples)	**2** (1-8)	**0 (0)**	**4.93 x 10^3** (0 –1.62 x 10^9)
Group III: 10-50 decoy cells (n = 14 samples)	**21** (10-48)	**26** **(**6-80)	**4.9 x 10^8** (7.08 x 10^6 – 1.32 x 10^9)
Group IV: >50 decoy cells (n = 13 samples)	**100** (50-318)	**84** (40 – 167)	**5.84 x 10^8** (3.65 x 10^7- 3.88 x 10^9)

*/10 hpfs= 40x high power field.

**/10 hpfs = 63,000x high power field.

*** = BK copies/ml

Table 2: Comparative Analysis of samples from patients with BKN (at time of initial biopsy diagnosis) versus transplant patients without BKN:

	BKN positive patients **N = 7** Median (range)	**BKN negative patients** **N = 31** Median (range)
Decoy Cells*	50 (10 – 318)	8 (0 – 150)
Negative staining EM**	62 (6 – 107)	4 (0 – 70)
Quantitative Urine PCR***	1.18×10^8 ($7.5 \times 10^6 – 1.65 \times 10^9$)	0 ($0 – 8.79 \times 10^8$)

*/10 hpfs = 40x high power fields

**/10 hpfs = 63,000x high power fields.

*** = BK copies/ml.

Selected References

1. Biel SS, Nitsche A, Kurth A, et al.: *Detection of human polyomaviruses in urine from bone marrow transplant patients: comparison of electron microscopy with PCR.* Clin Chem 2004, 50:306-12
2. Ding R, Medeiros M, Dadhania D, et al.: *Noninvasive diagnosis of BK virus nephritis by measurement of messenger RNA for BK virus VP1 in urine*. Transplantation 2002, 74:987-94
3. Drachenberg CB, Beskow CO, Cangro CB, et al.: *Human polyoma virus in renal allograft biopsies: morphological findings and correlation with urine cytology*. Hum Pathol 1999, 30:970-7
4. Drachenberg RC, Drachenberg CB, Papadimitriou JC, et al.: *Morphological spectrum of polyoma virus disease in renal allografts: diagnostic accuracy of urine cytology*. Am J Transplant 2001, 1:373-81
5. C. Drachenberg, H.H. Hirsch and J.C. Papadimitriou *et al., Cost efficiency in the prospective diagnosis and follow-up of polyomavirus allograft nephropathy*. Transplant Proc 2004, 36: 3028–3031
6. H.H. Hirsch, D.C. Brennan and C.B. Drachenberg et al.: *Polyomavirus-associated nephropathy in renal transplantation: interdisciplinary analyses and recommendation.* Transplantation 2005, 79**:** 1277–1286
7. Hirsch HH, Knowles W, Dickenmann M, et al.: *Prospective study of polyomavirus type BK replication and nephropathy in renal-transplant recipients*. N Engl J Med 2002, 347:488-96
8. Howell DN, Smith SR, Butterly DW, et al.: *Diagnosis and management of BK polyomavirus interstitial nephritis in renal transplant recipients*. Transplantation 1999, 68:1279-88
9. Leung AY, Chan M, Tang SC, et al.: *Real-time quantitative analysis of polyoma BK viremia and viruria in renal allograft recipients*. J Virol Methods 2002, 103:51-6
10. Nickeleit V, Bubendorf L, M. Z, et al.: *Polyomavirus-infected decoy cells in urine cytology specimens of renal allograft recipients: clinico-pathological considerations*. Mod Pathol 2002, 15:82A
11. Nickeleit V, Klimkait T, Binet IF, et al.: *Testing for polyomavirus type BK DNA in plasma to identify renal-allograft recipients with viral nephropathy*. N Engl J Med 2000, 342:1309-15
12. Nickeleit V, Singh, HK, Mihatsch, MJ.: *Polyomavirus nephropathy: morphology, pathophysiology, and clinical management.* Current Opinion in Nephrology and Hypertension 2003, 12:599-605
13. Papadimitriou JC, Drachenberg CB, Ravinder W, et al.: *BK virus in allograft nephropathy: ultrastructural features from tubular cell entry to lysis*. Am J Transplant 2003, 3:A317
14. Randhawa P, Ho A, Shapiro R, et al.: *Correlates of quantitative measurement of BK polyomavirus (BKV) DNA with clinical course of BKV infection in renal transplant patients*. J Clin Microbiol 2004, 42:1176-80

15. Singh H**,** Bubendorf L, Mihatsch MJ, Drachenberg C, Nickeleit V: *Urine Cytology Findings of Polyomavirus Infections* in: Ashan N, ed. Polyomaviruses. Eurekah, Georgetown, TX, 2005: Chap 13 [in press]
16. Hayat, M.A.: *Basic Techniques in Transmission Electron Microscopy.*Academic Press, Inc., Orlando 1986
17. Hayat, M.A. and Sara E. Miller: *Negative Staining.* McGraw-Hill Publishing Co., New York, 1990: 1-21

THE CONTRIBUTION OF QUANTITATIVE TECHNIQUES INCLUDING MORPHOMETRY TO RENAL DIAGNOSIS

M. Kashgarian, M.D.
Department of Pathology
Yale University School of Medicine
New Haven, Connecticut

Image analysis and stereological methods are essential tools in evaluating genetic diseases of the kidney and in experimental renal pathology in determining the phenotype of mutant and transgenic animals since the altered gene expression may demonstrate quantitative rather than obvious qualitative morphologic changes. Since cells, tissues, and organs are three dimensional structures usually studied in two dimensional sections, unbiased statistical stereological methods must be used for quantitative analysis of three dimensional changes in shape, number, volume and surfaces of specific structures such as cells, renal tubules or cysts. These stereological methods have been facilitated by computer assisted digital techniques. Design based stereology utilizes techniques in which no assumptions are made about the geometry , orientation or spatial distribution of the structures being studied. The only requirement is that the objects be unambiguously identifiable on parallel sections or successive focal planes. Changes in volume, surface and number of objects may be estimated using the principles of Cavalieri (Italian mathematician 1598-1642) for total quantities and Delesse for ratios (French geologist, C.R. Acad. Sci (Paris) 25:544, 1847) combined with a non selective sampling technique using the "disector " principle of Sterio (J. Micro 134:127-136, 1984). This method allows parameters to be estimated from the profiles of three dimensional objects in arbitrarily oriented parallel sections separated by a distance "t". For example, the volume of a certain class of objects is estimated by $V = t \cdot \sum$ Area (profiles). The advantage of combining the " disector" with the Cavallieri technique is that we do not need to know the exact slice thickness, "t" being estimated by the thickness of the specimen divided by the total number of slices. These unbiased stereological methods have been adapted to the study of a variety of tissues and organs including the kidney by Gunderson (J. Micro 151:3-21,1988, J. Micro 150:1-20,1988, J. Micro 164:247-61,1991). Gunderson has modified the "disector " concept to create the nucleator, fracionator and point sampling techniques (APMIS 96:379-94, 1998) as additional tools to increase efficiency of measurement. For volume analysis, a series of microscopic sections are taken from a series of slices of the affected tissues discarding the first and last slice. The areas of the interest selected by the test lattice are measured using computer assisted image analysis. Data is calculated using established statistical criteria and formulae. This method provides a highly efficient and unbiased design for measuring arbitrary objects in three dimensional space using two dimensional sectional images.

Digital Image Acquisition using integrated CCD cameras has greatly simplified the ability to perform quantitative analysis of electron micrographs. Digital imaging combined with computer based image processing systems such as the Public Domain Open Source Program at the NIH is called Image J, which includes length, perimeter and area measurements, particle counting and intensity measurements facilitates quantitative

electron microscopy. Macros specific to applications can further simply the process. The incorporation of steriologic perimeters including a non-selective sampling technique can be thus incorporated into a rapid assessment of basement membrane thickness, mitochondrial or glomerular volume, capillary perimeter and length and extent of podocyte effacement. These techniques while primarily used for research applications also have broad application in the clinical evaluation of renal biopsies. The most obvious is in the diagnosis of thin basement membrane disease. It also has been long applied to the detection of early diabetic glomeruloscelorsis and has proven value in assessing progression of that disease particularly in Type I diabetes. A new application is in the measurement of glomerular volume in renal allograft biopsies. There have been some suggestions that measurements of glomerular volume in protocol biopsies can provide important prognostic information relating to the development of chronic allograft nephropathy. It must be emphasized that simple unsupervised measurements can give incorrect results and that a systemized approach such as using the “disector” technique is necessary for accurate results.

PLASTICITY OF MESANGIAL CELLS: A BASIS FOR UNDERSTANDING PATHOLOGICAL ALTERATIONS

G. A. Herrera, M.D.
Department of Pathology
Louisiana State University Health Sciences Center, Shreveport, LA

The glomerular mesangial cells were first recognized as a distinct cell type by Zimmermann in 1933. Mesangial cells constitute approximately 30-40% of the total glomerular cell population. These mesangial cells spread from the hilum of the glomerulus in an arboreal pattern and are embedded in their own extracellular matrix. These cells have direct continuity and maintain close contact with cells that populate the juxtaglomerular apparatus. The mesangium is responsible for providing support to the entire glomerular structure and maintaining the glomerular capillaries open.

In a seminal paper exquisitely written and illustrated by Marilyn Farquhar and George E. Palade titled: "Functional evidence for the existence of a third cell type in the renal glomerulus" published in 1962, the authors provided for the first time evidence that the so-called deep cells of the glomerulus-mesangial cells- exhibited distinct morphological and functional characteristics that separated them from endothelial and epithelial glomerular cells. At the time the existence of this third type of glomerular cells was still being disputed and quite controversial. The authors went on to speculate that on the basis of the location of these cells and by virtue of their occasional phagocytic activity, the mesangial cells likely participated in the disposal and degradation of filtration residues and noted that these cells closely resembled capillary pericytes. It was pointed out that these morphological and functional characteristics clearly separated mesangial cells from other glomerular cell types. More than 40 years later the hypotheses of Farquhar and Palade have been proven to be absolutely correct and although our understanding of mesangial cells is far more complete we are still adding crucial information to the role that these cells play in health and disease.

The glomerular mesangium consists of resident mesangial cells and extracellular matrix. Two types of mesangial cells: a predominant smooth muscle-like cell with myofilaments and contractile properties and a second much less common phagocytic cell type (only about 3-10% of all mesangial cells) have been documented to be present in the normal mesangium. Morphologically the first type of mesangial cells show branching cytoplasmic processes with well developed filamentous network rich in actin and attachment plaques. The second mesangial cell type was felt to be derived from the bone marrow and has been shown to express Fc and C3 receptors. The normal mesangial matrix contains predominantly collagen IV but also has other extracellular matrix glycoproteins such as laminin and fibronectin, as well as proteoglycans including biglycan and decorin. Ultrastructurally, the mesangial matrix is seen to contain a dense network of microfibrils, which serve to anchor the mesangial cells. Mesangial cell functions are many and include regulation of capillary flow, maintenance of glomerular structure, production of vasoactive substances, cytokines and matrix components. Normal mesangial turnover is the result of a tightly controlled and dynamic equilibrium between the synthesis of new matrix and degradation and removal of the "old" matrix.

There are a number of key players that maintain equilibrium in the mesangial matrix in normal conditions. In essence, mesangial homeostasis is maintained by a balance of extracellular matrix production stimulated by transforming growth factor (TGF)-β and matrix destruction primarily resulting from activation of matrix metalloproteinases (MMPs) which are themselves maintained under control by tissue inhibitors of metalloproteinases (TIMPs), plasminogen activator inhibitor (PAI) and other non-specific inhibitors such as alpha-2 macroglobulin. Furthermore, changes in the amount and composition of the mesangial matrix can be associated with profound effects on the ability of mesangial cells to function properly. Any changes in these regulatory molecules leads to alterations in mesangial homeostasis and morphological expressions of disease that we use as diagnostic criteria. Thus, an appreciation of the mechanisms that determine the amount and composition of the mesangial matrix is of paramount importance to understand normal glomerular function and the results emanating from pathological changes.

One of the hallmarks of a great number of glomerulonephritis is the proliferation and activation of mesangial cells. Receptors have been described in mesangial cells that interact with a variety of stimuli and injurious agents leading to cellular alterations and if uncontrolled to pathologic results. Platelet-derived growth factor (PDGF)- beta (β) activation results in mesangial cell proliferation. Interestingly, TGF-β, the mesangial cell matrix rebuilder, is an anti-mitogenic factor for mesangial cells. Mesangial cells are very active metabolically synthesizing an array of substances such as cytokines which result in stimulation of cellular proliferation, cell shape changes, recruitment of inflammatory cells, including macrophages and monocytes, among many others. The interactions between cytokines and mesangial cells result in many of the alterations of the mesangial matrix that occur during the progression of immune and non-immune complex mediated glomerulopathies. Both resident and non-resident cells, including inflammatory cells, secrete factors that stimulate mesangial cell proliferation and matrix production, alter glomerular basement membrane permeability, and regulate blood flow. The native mesangial matrix is altered by the deposition of increasing quantities of normally expressed mesangial matrix components as well as other extracellular matrix proteins, which are not normally present in the mesangium. The mesangial matrix once initially altered, engages in a pathologic cycle which enhances further mesangial matrix expansion and further departure in composition from normal. If the pathologic process is not controlled, glomerulosclerosis occurs, resulting in a markedly altered mesangium morphologically and biochemically which is impossible to extremely difficult to repair and return to normal. Mesangial cells “trans” or “de” differentiate in response to injury. El Nahas refers to a change from the pericyte (smooth muscle) phenotype (“mesangiocyte”) to the embryonic myofibroblastic phenotype (“mesangioblast) as a characteristic response to mesangial injury. In the process, the mesangial cells acquire a range of cytoskeletal proteins, including alpha-smooth muscle actin. This process has been considered to reflect reverse embryogenesis of adult and mature mesangial cells. Change to the myofibroblastic phenotype eventually results in corresponding alterations in the mesangial matrix. These mesangial cells with myofibroblastic phenotype synthesize an array of different extracellular matrix proteins not normally present in the mesangium and difficult to destroy, including collagens I and III (interstitial/fibrillary collagens). The switch by mesangial cells from the production of collagen IV to

interstitial, fibrillary type of collagens has major pathologic consequences and represents a major factor in progression to glomerulosclerosis, as the glomeruli lack the necessary machinery (i.e. MMPs) to degrade the newly synthesized abnormal matrix components. Recent evidence supports that mesangial cells transform from the normal smooth muscle-like phenotype to a macrophage phenotype when exposed to certain injurious agents and engage in active phagocytosis. The plasticity of mesangial cells is responsible for glomerular damage, including mesangial matrix replacement, scarring and remodeling.

This presentation will discuss the importance of mesangial cells and matrix in maintaining normal glomerular structure and function (homeostasis) and also will address how the plasticity of these cells influences pathological glomerular events, repair and scarring. Our much more sophisticated understanding of mesangial cell behavior and mesangial matrix biology provides very useful information to help the design of new therapeutic approaches to the treatment of renal diseases. The potential for bone marrow-derived cells to differentiate into glomerular mesangial cells and repopulate damaged mesangium represents an exiting area of research that may lead to novel therapeutic strategies to address irreversible glomerular damage.

References:

1. Baud L, Perez J, Ardaillou R: Dexamethasone and hydrogen peroxide production by mesangial cells during phagocytosis. Am J Physiol 250:F596-604, 1986.
2. Berfield AK, Abrass CK: IGF-1 induces foam cell formation in rat glomerular mesangial cells. J Histochem Cytochem 50:395-403, 2002.
3. El Nahas AM: Plasticity of kidney cells: role in kidney remodeling and scarring. Kidney Int 64:1553-1563, 2003.
4. Farquhar MG, Palade GE: Functional evidence for the existence of a third cell type in the renal glomerulus. Phagocytosis of filtration residues by a distinctive “third” cell. J Cell Biol 13:55-87, 1962.
5. Gabbiani G: Evolution and clinical implications of the myofibroblast concept. Cardiovasc Res 38:545-548, 1998.
6. Holthofer H, Sainio K, Miettinen A: The glomerular mesangium: studies of its developmental origin and markers in vivo and in vitro. APMIS 103:354-366, 1995.
7. Imasawa T, Utsunomiya Y, Kawamura T, et al: The potential of bone marrow-derived cells to differentiate to glomerular mesangial cells. J Am Soc Nephrol 12:1401-1409, 2001.
8. Isaac J, Kerby JD, Russell WJ, et al: In vitro modulation of AL-amyloid formation by human mesangial cells exposed to amyloidogenic light chains. Amyloid: Int J Exp Clin Invest 5:238-246, 1998.
9. Ito T, Suzuki A, Imai E, et al: Bone marrow is a reservoir of repopulating mesangial cells during glomerular remodeling. J Am Soc Nephrol 12:2625-2635, 2001.
10. Johnson RJ, Iida H, Alpers CE, et al: Expression of smooth muscle cell phenotype by rat mesangial cells in immune complex nephritis. α-Smooth muscle actin is a marker of mesangial cell proliferation. J Clin Invest 87:847-858, 1991.
11. Johnson RJ, Floege J, Yoshimura A, et al: The activated mesangial cell: a glomerular "myofibroblast"? J Am Soc Nephrol 2:S190-197, 1992.
12. Keeling J, Teng J, Herrera GA: AL-amyloidosis and light chain deposition disease light chains induce divergent phenotypic transformations of human mesangial cells. Lab Invest 84:1322-1338, 2004.
13. Keeling J, Herrera GA: Matrix metalloproteinases and mesangial remodeling in light chain-related glomerular damage. Kidney Int: 68:1590-1603, 2005.
14. Kim SI, Han DC, Lee HB. Lovastatin inhibits transforming growth factor-β 1 expression in diabetic rat glomeruli and cultured rat mesangial cells. J Am Soc Nephrol 11:80-87, 2000.
15. Kreisberg JI, Venkatachalam M, Troyer D: Contractile properties of cultured glomerular mesangial cells. Am J Physiol 249:F457-463, 1985.
16. Latta H, Maunsbach AB, Madden SC: The centrolobular region of the renal glomerulus studied by electron microscopy. J Ultrastruct Res 4:455-472, 1960.
17. Martin J, Eynstone L, Davies M, et al: Induction of metalloproteinases by glomerular mesangial cells stimulated by proteins of the extracellular matrix. J Am Soc Nephrol 12:88-96, 2001.

18. Mori T, Bartocci A, Satriano J, et al: Mouse mesangial cells produce colony-stimulating factor-1 (CSF-1) and express the CSF-1 receptor. J Immunol 144:4697-4702, 1990.
19. Moura IC, Arcos-Fajardo M, Sadaka C, et al: Glycosylation and size of IgA1 are essential for interaction with mesangial transferrin receptor in IgA nephropathy. J Am Soc Nephrol 15:622-634, 2004.
20. Ooi BS, Cohen DJ, Veis JH: Biology of the mesangial cell in glomerulonephritis--role of cytokines. Proc Soc Exp Biol Med 213:230-237, 1996.
21. Patel K, Harding P, Haney LB, et al: Regulation of the mesangial cell myofibroblast phenotype by actin polymerization. J Cell Physiol 195:435-445, 2003.
22. Russell WJ, Cardelli J, Harris E, et al: Monoclonal light chain-mesangial cell interactions: Early signaling events and subsequent pathologic effects. Lab Invest 81:689-703, 2001.
23. Saito K, Shimizu F, Sato T, et al: Modulation of human mesangial cell behaviour by extracellular matrix components--the possible role of interstitial type III collagen. Clin Exp Immunol 91:510-515, 1993.
24. Schlondorff D: The glomerular mesangial cell: an expanding role for a specialized pericyte. FASEB J 1:272-281, 1987.
25. Schreiner GF: The mesangial phagocyte and its regulation of contractile cell biology. J Am Soc Nephrol 2:S74-82, 1992.
26. Sedor JR, Konieczkowski M, Huang S, et al: Cytokines, mesangial cell activation and glomerular injury. Kidney Int 43:S65-S70, 1993.
27. Silver BJ, Jaffer FE, Abboud HE: Platelet-derived growth factor synthesis in mesangial cells: induction by multiple peptide mitogens. Proc Natl Acad Sci U S A 86:1056-1060, 1989.
28. Teng J, Russell WJ, Gu X, et al: Different types of glomerulopathic light chains interact with mesangial cells using a common receptor but exhibit different intracellular trafficking patterns. Lab Invest 84:440-451, 2004.
29. Zimmerman KW: Über den Bau des Glomerulus der Säugerniere: Weitere Mitteilungen. Z Mikrosk Anat Forsch 32:176-278, 1933.

REVIEW OF AUTOIMMUNE (LUPUS-LIKE) GLOMERULONEPHRITIS IN MURINE MODELS

John Hicks, MD
Department of Pathology
Texas Children's Hospital and Baylor College of Medicine
Houston, TX

Over the past decade, animal models for immune complex glomerulonephritis have been developed in an attempt to understand this disease process. The majority of the murine models have been created to mimic glomerulonephritis associated with systemic lupus erythematosus (SLE, Table 1). In humans, renal involvement occurs to a variable degree in up to 50% of affected individuals. The extent of lupus nephritis (LN) may range from microhematuria and mild proteinuria to nephrotic syndrome to progressive renal failure and ultimately end-stage renal disease. The glomeruli, tubules and vessels may be affected to a variable degree. Immune complex deposits within the glomeruli and vessels, in addition to tubular basement membranes, are detected by "full-house" immunofluorescence (immunoreactivity with IgA, IgG, IgM, C3, C4, C1q, MAC, fibrinogen) and electron dense deposits within the mesangium, subendothelium, subepithelium and within glomerular basement membranes. Diffuse proliferative glomerulonephritis and immune complex deposits lead to distinct patterns that allow for classification of LN (WHO Class I->V LN). LN may undergo periods of remission and exacerbation. With appropriate treatment, it is possible to transform a more severe form of LN to a less severe morphologic LN pattern. The development of animal LN models has provided certain insights into the human form of LN.

Murine Models of Lupus Nephritis

There are many different murine SLE models (Table 1). Certain murine strains have inherited susceptibility to SLE-like symptoms and manifestations, and develop severe systemic autoimmunity spontaneously with features resembling SLE. These models help to eliminate the heterogeneity of the disease process that occurs in humans and allow for a more systematic evaluation of SLE and LN in a relatively well-defined background. This allows for discovery of pathophysiologic factors, immune regulators and candidate genes in SLE and LN.

The most commonly used murine strains for investigating SLE are MRL/MpJ, MRL/MpJ-lpr, NZB hybrids and BXSB/MpJ animals. These murine strains inherit an autoimmune susceptibility and develop diffuse proliferative glomerulonephritis, immune complex and complement deposits, mononuclear cell infiltrates, interstitial nephritis and progressive renal failure. The MRL/MpJ-lpr (MRL/lpr) strain is generated due to a retroviral transposon insertion mutation (*lpr* gene) on chromosome 19 in the gene encoding for the Fas antigen (CD95). Fas is a cell surface receptor that mediates apoptosis. With disruption of Fas function and expression, lymphocyte apoptosis is impaired and allows for lymphoproliferation (lpr). When the *lpr* mutation is superimposed upon the MRL autoimmune background, a severe SLE phenotype occurs in the affected animal. These animals also produce autoantibodies (anti-dsDNA, anti-ssDNA, anti-nuclear antibodies [ANA], anti-GP70). SLE occurs at an early age in a very severe form with 50% mortality by 6 months of age. These animals also have a massive

proliferation of T-cells, characterized by their CD4-, CD8-, TCR alpha-beta+, and B220+ immunophenotype. A similar phenotype is seen when a mutation in the *gld* gene (generalized lymphoproliferative disease) occurs. This gene mutation occurs in the extracellular domain of the Fas ligand (FasL, chromosome 1) and results in lack of binding of Fas to its ligand (FasL). New Zealand Black mice (NZB) when crossed with New Zealand White mice (NZW) develop severe lupus-like autoimmunity. Immune complex glomerulonephritis occurs secondary to the induction of IgG autoantibody production. The BXSB/MpJ (BXSB) strain also serves as an SLE and LN murine model. Interestingly, males develop more severe disease than females with 50% mortality by age 6 months for males and by 20 months for females. The difference in severity of disease and mortality is ascribed to the *Yaa* gene (Y-chromosome-linked autoimmune accelerator) located on the BXSB Y-chromosome. This gene is thought to potentiate selective immune responses.

In addition to these classic spontaneous murine models for SLE, there are many other models that may be used for induction of an SLE-like phenotype (Table 1). These models may be generated by mutations in classic murine lupus strains, gene deletions, transgene insertions, spontaneous gene mutations, gene-targeted deletions, induction of gene overexpression, drug and metal salt induction, or immunization with various agents.

Candidate Genes in Systemic Lupus Erythematosus

It is well known that SLE has a certain genetic basis. Familial clustering studies have shown that SLE has a sibling risk ratio similar to that for other autoimmune diseases, such as diabetes type 1 and rheumatoid arthritis. Twin studies have indicated a 10-fold concordance for SLE in monozygotic versus dizygotic twins. Genome linkage investigations have revealed 7 susceptibility loci at 1q23-24, 1q41-42, 2q37, 4p15-16, 6p11-22, 16q12-13 and 17p13. Another 20 loci are suggestive of SLE linkage.

At least 5 susceptibility loci have been identified both in human and murine SLE (Table 2). These include CRP/SAP (c-reactive protein/serum albumin P component at 1q23.2), DNASE1 (16q13.3), C1q (1p36), Fc-gamma RIIA/IIA (1q23) and PDCD1 (2q37.3). CRP/SAP is the major acute phase protein generated following inflammation and injury. This protein binds apoptotic products, including cellular matrix and nuclear antigens, to promote opsonization and clearance of these degraded particles. This activity avoids the development of autoantibodies to these degraded particles. In human SLE, there is a minimal to absent acute phase response to inflammation and injury. A CRP/SAP knockout murine model has been shown to develop autoimmunity and glomerulonephritis, purportedly due to lack of clearance of chromatin. The resultant autoantibodies become deposited within the kidneys. DNASE1 is involved in removal of potential autoantigens, as well. SLE patients have reduced serum DNASE1 activity. DNASE knockout mice have increased autoantibody production against nuclear antigens, in particular ssDNA and nucleosomes. C1q initiates the classical pathway in the complement cascade. Homozygous hereditary C1q deficiency is considered to be a risk factor for SLE development, with 90% of those acquiring SLE at an early age. Low serum levels of C1q are predictive of proliferative LN. C1qa knockout mice have high ANA titers and anti-histone antibodies, and 25% have glomerulonephritis. Fc-gamma receptors have also been implicated in autoimmunity. The murine genes *Nba1* and *Sle1* contain two Fc-gamma receptors that are linked to LN. Fc-gamma receptor 2 and 3 are considered most important in linkage to SLE. The Fc-gamma receptors are critical to clearance of antibodies and immune complexes. Fc-gamma receptor IIa

is the major receptor class for IgG2. Mutations in this receptor leads to anti-dsDNA autoantibody production, due to delayed or lack of clearance of dsDNA-IgG2 immune complexes. Both IgG2 and IgG3 in humans and murine models have been ascribed a pathogenic role in kidney disease. Low binding of the F/V158 allele of the Fc-gamma receptor IIa has been associated with LN. Knockout murine models indicate that both Fc-gamma receptor 2 and 3 are involved with disease initiation and immune complex deposition in the kidneys. PDCD1 is present at the SLEB2 locus, and is an inhibitory transmembrane receptor that down regulates lymphocyte proliferation and cytokine secretion. Its function is important for maintaining peripheral tolerance. Loss of function results in breakdown in tolerance and lymphocyte hyperactivity. Knockout mice develop spontaneous LN and arthritis.

There are several murine SLE susceptibility genes that are yet to be proven in the development of human SLE (Table 2). These include MHC Class II genes, Y-linked accelerator of autoimmunity (*Yaa*, Y chromosome*), lpr* (Fas, chromosome 19), *gld* (FasL, chromosome 1) and *me* (motheaten, SHP-1, chromosome 6, protein tyrosine phosphatase). MHC Class II correlates strongly with LN in several mouse strains. This is due to the role of MHC Class II members in antigen presentation. *Yaa*, *lpr* and *gld* accelerate LN in mouse strains that have underlying spontaneous, inherited autoimmunity susceptibility (MRL/MpJ, NZBxNZW, BXSB). Interestingly, *lpr* and *gld* induce autoantibody production and autoimmunity in non-autoimmune mouse strains. This is due to the fact that Fas and FasL interactions are responsible for peripheral elimination of autoreactive B and T cells via apoptotic pathways. The apoptotic pathway is critical for maintaining normal immune homeostasis. There are several other murine susceptibility loci linked to murine LN (Table 2). *Nba-1* has a strong association with renal disease and mortality, and induces elevated antinuclear antibody and hypergammaglobulinemia levels. Early mortality and glomerulonephritis has been linked to *Lbw1, Lbw 2* and *Lbw6*. *Sle1, Sle2* and *Sle3* are associated with anti-dsDNA Ig and glomerulonephritis. *Lbw7* leads to anti-chromatin antibody production and glomerulonephritis. Several genes contribute to renal disease susceptibility in MRL mice. These include *Lrdm*, *Lmb1, Lmb 2, Lmb3,* and *Lmb4.* Anti-dsDNA antibodies are associated with these gene susceptibility loci in MRL mice. *Lyn* is an Src protein-tyrosine kinase involved with negative signaling in lymphocytes. Mutation in this gene results in anti-DNA antibodies and immune complex glomerulonephritis. Several homologous-induced gene deletions (knockout and transgenic models) in normal background mice lead to LN and autoantibody production (Table 3). Other potential candidate genes are those that participate in apoptosis pathways, lymphocyte signaling, T cell selection, cell-to-cell adhesion and antigen presentation, macrophage function, cytokine expression, and negative regulation of lymphocyte activation.

Certain gene knockouts in lupus susceptible mice result in improved survival, reduction in autoantibody production and less severe glomerulonephritis (Table 3). These genes encode for signal transduction pathways, growth factors, accessory molecules, cytokine and chemokine pathways, and the complement cascade. Their functional importance is emphasized by the profile of chemokines, cytokines and growth factors produced by renal parenchymal cells (Table 4). Most of these participate as proinflammatory molecules and recruit leukocytes. Several have a putative role in expression of fibrotic growth factors and may lead to glomerulosclerosis and interstitial fibrosis. Others regulate and activate lymphocytes and are essential in leukocyte adhesion and emigration of leukocytes from the vascular spaces into tissues.

Adhesion Molecules in Inflammation and Glomerulonephritis

Several vasculitic diseases are associated with dysregulation of adhesion molecules (Table 5). These diseases include those that have been classified as immune complex disorder (SLE, rheumatoid arthritis), anti-neutrophil cytoplasmic antibody disorders (Churg-Straus syndrome), and T-cell response and granuloma disorders (giant cell arteritis). This is not surprising because the inflammatory process begins with adhesion of leukocytes within the vascular space and transmigration and emigration of the activated leukocytes into tissues.

There are 3 major families of adhesion molecules involved in the inflammatory process (Table 6): selectins, integrins, and the immunoglobulin superfamily of adhesion receptors. These proteins mediate cell-cell interactions during normal immune and inflammatory responses. This includes leukocyte-to-leukocyte interactions, and leukocyte adhesion to endothelial cells, smooth muscle, extracellular matrix, and interstitial cells. The major role of adhesions molecules is to promote leukocyte recruitment from the vascular space into tissues in response to inflammatory signaling.

P-Selectin (CD62P) is synthesized by megakaryocytes (platelets) and endothelial cells, and is rapidly expressed in response to certain agonists (histamine, thrombin, Table 6). Its ligands are PSGL-1, CD24 and CD15. L-Selectin (CD62L) is constitutively expressed on the surfaces of all leukocytes. Its ligands are GLYCAM-1, CD34, MAdCAM-1 and CD15. E-Selectin (CD62E) is synthesized by activated endothelial cells in response to IL-1, TNF-alpha and beta, and LPS. Synthesis requires 4 to 6 hours and E-Selectin is not immediately available. Its ligands are ESL-1, PSGL-1 and CD15. Selectins are composed of several different domains that participate in leukocyte adhesion (Table 6). Selectins mediate the first steps in leukocytes adhesion, initial leukocyte recruitment, rapid bond formation to promote adherence, rapid dissociation to facilitate leukocyte rolling, and have a favorable free energy to resist shear forces in the bloodstream.

Integrins are heterodimers proteins with a common beta subunit that is covalently attached to different alpha subunits (Table 6). These proteins are constitutively expressed on leukocytes, endothelial cells and other cell types. Integrins mediate cell-cell and cell-matrix interactions in response to an inflammatory stimulus. LFA-1 (CD11a/CD18) is a member of the beta-2 integrin family (CD18 integrins) and is expressed on neutrophils, lymphocytes and macrophages. Its ligands are ICAM-1, ICAM-2 and ICAM-3. It is induced by antigen stimulated T-cell priming. MAC-1 (CD11b/CD18) is another member of the beta 2 integrin family and is found with neutrophils and macrophages. Its ligands include ICAM-1, ICAM-2, Fc, iC3b, Factor X and fibrinogen. A beta-1 integrin family member is VLA-4 (CD49d/CD29) and it has beta-1 and alpha-4 subunits. It is expressed on granulocytes (primarily), lymphocytes and macrophages. Its ligands are VCAM-1 and fibronectin. Integrins participate in firm adhesion of leukocytes, extravasation of leukocytes from the vascular space and emigration into and through tissues in response to inflammatory signaling.

The members of the immunoglobulin superfamily (ICAM-1, ICAM-2, VCAM-1, PECAM-1) participate in firm adhesion of leukocytes and extravasation of leukocytes, in concert with the integrins (Table 6). This family of adhesion molecules is characterized by a series of repeating extracellular IgG-like domains, a transmembrane region and a short cytoplasmic tail. All members of this group are expressed on activated endothelial cells, with PECAM-1 being also found on polymorphonuclear cells and macrophages. The ligands for ICAM-1 (CD54) and ICAM-2 (CD102) are LFA-1 (CD11a/CD18) and Mac-1 (CD11b/CD18). The ligand for

VCAM-1 (CD106) is the integrin VLA-4 (CD49d/CD29). PECAM-1 (CD31) interacts with other PECAM-1 proteins and acts as its own ligand.

The inflammatory process begins with activation of leukocytes to an immunologic or inflammatory stimulus (Table 6). Leukocyte activation results in interaction of selectins expressed on the leukocytes with their ligands, as well as integrins and the Fc-gamma receptor. The initial stage of leukocyte adhesion to the vessel wall (leukocyte rolling) is mediated by selectins and the integrin VLA-4. Firm adhesion of the leukocytes to the endothelium and vessel wall components results from interactions between integrins (LFA-1, Mac-1) and members of the immunoglobulin superfamily of adhesion receptors (ICAM-1, ICAM-2, VCAM-1). Leukocyte extravasation and emigration into tissues is secondary to interactions between integrins (LFA-1, Mac-1) and adhesion molecule receptors (ICAM-1, ICAM-2 VCAM-1, PECAM-1).

Of particular interest is the fact that both selectins and integrins are expressed on many of the glomerular cells, tubular epithelium, venules, and interstitial cells, particularly when glomerulonephritis is present (Table 7). This may, in part, explain the vulnerability of the glomerulus and other components of the kidney to immune-mediated disease processes.

Certain experimental strategies to inhibit leukocyte adhesion have been developed to attenuate the effects of immunologic and inflammatory mediated disease. Monoclonal antibodies against adhesion epitopes, soluble adhesion molecule fragments or analogs (decoys), anti-sense oligonucleotides to inhibit adhesion molecule synthesis, and regulation of endogenous anti-inflammatory networks have been investigated with considerable success in animal models of inflammatory diseases. Of interest are renal diseases that may be affected by inhibition of adhesion molecule synthesis or function. In animal models, inhibition of adhesion molecule synthesis or function has shown great promise with acute immune complex glomerulonephritis, crescentic glomerulonephritis, hereditary tubulointerstitial nephritis, lupus glomerulonephritis, allograft rejection, and ischemic acute renal failure. Application of these regimens to human immune and inflammatory mediated diseases may become a reality in the not too distant future.

Modulation of Murine Lupus Nephritis

During the past decade, the effects of deletions in adhesion molecule receptors and integrins have been evaluated using a murine lupus nephritis model (MRL/Fas^{lpr}). The results from these studies provide insight into the role of leukocyte trafficking and potential immune modulation therapy for clinical management of lupus nephritis.

ICAM-1 Deletion and Murine Lupus Nephritis

A comparison of mice with lupus nephritis (Fas) and those with ICAM-1 knockout (Fas/ICAM-1) proved to be quite enlightening with respect to survival, serology and renal histopathology (Table 9). Median survival was dramatically different for Fas mice versus Fas/ICAM-1. Survival was increased by 1.8-fold. BUN was reduced by two-thirds in the ICAM-1 knockout mice, while IgG levels were decreased by about one-quarter. For reference, BUN in wild type mice is typically 25 mg/dL. Anti-dsDNA levels were lessened by about 50%. These findings were statistically significant, and it was evident that ICAM-1 deletion protected against early lethality compared with Fas mice. The histopathologic evaluation demonstrated marked differences between the two groups at 22 weeks of age and at necropsy of mice that died during the study. Kidneys from Fas mice showed marked periglomerular and interstitial inflammatory infiltrates. The glomeruli possessed thickened capsules and marked mesangial

hypercellularity and mesangial matrix increase. Tubular atrophy was readily identified. In contrast, the Fas/ICAM-1 mice had a moderate decrease in mesangial cellularity and matrix accumulation, and a moderate decrease in interstitial inflammatory infiltrates. Tubular atrophy, although present, was less frequent. Kidney disease progression in those animals that died during the study was considerably greater for the Fas mice than that for the Fas/ICAM-1 mice. In fact, diffuse global sclerosis was noted in the deceased Fas mice, but not in the deceased Fas/ICAM-1 mice. Ultrastructural examination of the kidneys at 22 weeks and at necropsy of mice that died during the study revealed greater degrees of electron dense mesangial deposits in the Fas group than in the Fas/ICAM-1 group at both the 22 week age period and in those animals that died during the study. Immune modulation of lupus nephritis with ICAM-1 deletion in Fas mice was evident and affected overall survival, serology and progression of kidney disease. ICAM-1 deficiency may inhibit leukocyte activation, and thereby reduce vasculitis.

Beta-2 Integrin Deletion and Murine Lupus Nephritis

The role of beta-2 integrins in modulation of lupus nephritis (MRL/Fas^{lpr}) has been investigated by knockout of CD18 (CD18/Fas). Deletion of CD18 results in severe or total deficiency in the beta-2 integrins, including LFA-1 (CD11a/CD18), Mac-1 (CD11b/CD18), P150/95 (CD11c/CD18) and Alpha-D2 (CD11d/CD18). As noted previously, integrins are intimately involved in leukocyte adhesion and transmigration from the vasculature to the site of inflammation. CD18 inhibition profoundly reduces leukocyte emigration into inflamed tissue sites. With CD18/Fas mice, significant reductions in lymphadenopathy and vasculitis were found. Serology for anti-dsDNA, anti-ssDNA and IgG were significantly reduced with the CD18/Fas animals. Histopathology of the kidneys was compared among wild type, Fas and CD18/Fas mice at 20 and 28 weeks of age. The Fas mice had considerable endocapillary proliferation in a diffuse pattern when compared with both the wild type and CD18/Fas mice. The CD18/Fas mice had a minimal to mild endocapillary proliferation. Electron microscopy showed diffuse and confluent mesangial electron dense deposits with the Fas group. In contrast, infrequent to rare isolated mesangial deposits were identified with the CD18/Fas group. The wild type mice lacked immune deposits. Overall, CD18 deletion in murine lupus nephritis attenuated lymphadenopathy, vasculitis, and autoantibody production, as well as, substantially reducing glomerulonephritis. CD18 deficiency inhibits or substantially lessens adhesion and transmigration of leukocytes into tissues, and would appear to modulate leukocyte mediated autoimmune and immune complex glomerulonephritis.

LFA-1 and Mac-1 Deletions and Murine Lupus Nephritis

In order to understand the contribution of the integrins LFA-1 (CD11a/CD18) and Mac-1 (CD11a/CD18), Fas mice with deletions of CD11a (LFA-1/Fas) and deletion of CD11b (Mac-1/Fas) were generated. Median survival was dramatically extended with deletion of LFA-1 (41 weeks) compared with the Fas (24 weeks) and Mac-1/Fas (22 weeks) groups (Table 9). BUN was substantially reduced in the LFA-1/Fas group, and was similar to that expected for wild type mice (25 mg/dL). Both Fas and Mac-1/Fas mice had similar high BUN levels. Autoantibodies (anti-dsDNA, anti-ssDNA, IgG, IgM) were significantly reduced with LFA-1/Fas mice compared with Fas and Mac-1/Fas mice. Lymphadenopathy and cutaneous vasculitis were reduced with the LFA-1/Fas mice. Mac-1/Fas mice had exaggerated lymphadenopathy and similar cutaneous vasculitis as Fas mice. Kidneys were examined at 20 weeks with all groups and evaluated using the Austin lesion scoring system (glomerular cellularity, necrosis, crescent

formation, neutrophil accumulation, capillary basement membrane changes, mesangial sclerosis, capsular fibrosis, interstitial mononuclear inflammation, tubular atrophy, interstitial fibrosis). The Austin lesion scores were substantially different between LFA-1/Fas (4.9) and both Mac-1/Fas (11.9) and Fas (16.8). The Austin lesion score for Mac-1/Fas was moderately less than that for Fas, but considerably greater than that for LFA-1/Fas. The Fas and Mac-1/Fas kidneys appeared similar with hypertrophic glomeruli with a moderate increase in mesangial cellularity and matrix. Basement membrane reduplication and thickening was present. Focal necrosis and fibrin deposition were also noted. In contrast, LFA-1/Fas kidneys had only a mild increase in mesangial cellularity and matrix. The glomeruli tended to be hypertrophic, but lacked focal necrosis or fibrin deposition. Upon ultrastructural examination, Fas and Mac-1/Fas had abundant confluent electron dense deposits within the mesangium, subendothelium, and glomerular basement membranes. There were increased mesangial cells and matrix. With LFA-1/Fas kidneys, only small paramesangial and membranous electron dense deposits were found. Mesangial cells and matrix in LFA-1/FAS kidneys were decreased compared with Fas and Mac-1/Fas kidneys. It appears that LFA-1 plays an important role in murine lupus nephritis and abrogating its function by deletion of LFA-1, inhibition of LFA-1 (lovastatin selectively inhibits LFA-1 or anti-LFA1 antibodies) or blocking its adhesion molecule receptors (ICAM-1, ICAM-2, ICAM-3) may prove to be beneficial in reducing the severity of lupus nephritis.

Novel and Potential Therapy for Immune Complex Glomerulonephritis

Although certain standard therapies have been available for decades, only recently have novel therapies been discovered for glomerulonephritis (Table 10). The development of novel therapies have come to fruition based upon translational research involving animal models of glomerular diseases with confirmation of the findings in the corresponding human disease. These novel treatment agents can be divided into immune/inflammatory agents with subtyping as immune response (LJP 394, anti-CD20), costimulation (anti-CD154, CTLA4, anti-CD80, anti-CD86), immune effector (anti-CD5) and cytokine/chemokine (STI571, anti-TNF, IL-1a) agents. Monoclonal antibodies have been introduced into clinical practice that augment or supplant the standard therapy for glomerulonephritis. Antibodies to adhesion molecules (integrins, ICAM-1) and cell cycle components (trans-retinoic acid, R-roscovitine) are available for clinical use. Of particular interest is the potential to avoid interstitial fibrosis by modulating various growth factors responsible for fibrosis and epithelial-mesenchymal transition (hepatocytes growth factor, bone morphogenic protein-7). Other novel therapies include bone marrow transplantation, in an attempt to replace leukocytes that have mutations with leukocytes that have normal function. Nucleoside analogs have great promise in treating glomerulonephritis and potentially avoiding progression of disease (fludarabine, 2-CdA). Certain agents are directed toward controlling the proliferation of aberrant T-cells (anti-CD4, CD5-Plus). Anti-idiotype and competitive proteins provide a means of “turning off” the vicious cycle of injury that is self-perpetuating in autoimmune diseases. Introduction of novel anti-inflammatory drugs may allow for abrogation or attenuation of the inflammatory process (thromboxane receptor antagonist).

Directing therapy toward B cells seems to be promising as well (Table 10). There are several antibodies directed toward B cells that are currently in clinical use with excellent results in controlling the progression of glomerulonephritis (anti-CD20, anti-CD40L). Other agents act to block activation of surface receptors and their ligands on B lymphocytes (CTLA4/Ig), as well as blocking T and B cell lymphocyte interactions (CTLA4Ig & anti-CD40L). The proliferation and differentiation of B cells may be inhibited effectively (anti-BLys). Induction of peripheral

tolerance with anti-dsDNA producing B cells and a reduction of anti-dsDNA may be induced with LJP-394. Anti-IL10 blockade of B cell mediators may be accomplished. B cell inhibition and reduction in autoantibodies is possible with anti-Interferon gamma. Inhibition of the complement complex attack system may occur with administration of anti-C5b monoclonal and anti-C3 antibodies.

It is quite obvious that it will take some time to determine the effectiveness of these novel agents in prevention and treatment of immune complex glomerulopathies. With additional genomic and proteomic discovery, other novel agents will emerge as susceptibility genes and their proteins become characterized. It is anticipated that additional biologic based therapies will rapidly evolve from the laboratory to clinical practice.

Table 1: Systemic Lupus Nephritis: Experimental Murine Models

- Classic Spontaneous Murine Lupus: Inherited Susceptibility
  - MRL/MpJ & MRL/MpJ-lpr/lpr Strain
  - NZB/NZW Strain
  - BXSB/MpJ Strain
- Mutant Variants of Classic Murine Lupus
  - BXSB/MpJScr-II/III Strain
  - NZM2410 Strain
  - SCG/Kj Strain
  - (NZWxBXSB)F1 Strain
  - Gene Deletions in MRL/lpr-lpr
    - Jh (B cell deficient), IFN-gamma, Beta2-microglobulin (MHC I deficient)
    - TCR alpha, TCR beta, TCR gamma/delta, MHC Class II, IFN-gamma receptor, IL-4, ICAM-1, CD40L
  - Transgenes
    - MHC Class II-E alpha in BSXB
    - IL-4 with Ig Promoter in NZBXC57BL/6,Yaa)F1
- Novel Mutant Murine Lineages: Single Gene Alterations
  - Gene Deletion Models (knockouts)
    - Spontaneous Mutations
      - *lpr* (lymphoproliferation)
      - *gld* (generalized lymphoproliferative disease)
      - *me* (motheaten)
      - *Yaa* (Y-chromosome-linked accelerator or autoimmunity
    - Gene-Targeted Deletions
      - *lyn*
      - TGF-beta1
- Novel Mutant Murine Lineages
  - Gene Overexpression Models (transgenes)
    - Fli-1
    - Bcl-2
    - Autoantibody Transgenes: alpha-DNA, alpha-RBC, alpha-Ig, alpha-laminin
    - IL-4
    - IFN-gamma
- Classical Investigator-Induced Murine Lupus
  - Drug and Metal Salt Induced Lupus
    - D-penicillamine
    - Procainamide
    - Mercury Salts
    - Gold Salts
  - Chronic Graft vs Host Disease
- Additional Models of Induced Murine Lupus
  - Pristane Administration
  - Immunization with DNA/Protein Complexes
  - Immunization with anti-DNA Idiotype or Anti-Idiotype Ig

Table 2: Susceptibility Loci in Human and Murine Systemic Lupus Erythematous

Gene	Human	Murine (chromosome:cM)	Murine Linkage Region
CRP/SAP	1q23.2	1:94.2	Sle1/Nba2
DNASE-1	16q13.3	16:1.7	-----
C1q	1p36	4:66.1	Nba1
Fc-gamma RIIA/IIA	1q23	1:92.3	Nba2
PDCD1	2q37.3	1D	Bxs3

Murine Susceptible Genes in Lupus Glomerulonephritis

Susceptibility Gene	Chromosome
FasL (*gld*)	1
SHP-1 *(me*)	6
MHC	17
Fas (*lpr*)	19
Yaa	Y

Murine Susceptible Loci In Lupus Glomerulonephritis

	(chromosome:cM)
Sle1	1:87.9
Nba2	1:92.3
Sle2	4:44.5
Lbw2	4:59.0
Nba1	4.67.2
Lmh1	4:69
Lrdm1	7:6.0
Sle3	7:28.0
Lmb4	10:51.0
Lrdm2	12:27.0
Lprm3	14:44.0
Nwa1	16:38.0
Lbw6	18:47.0
Cgnz1	D1Mit15-D1Mit37
Agnz1	D1Mit37-M1Mit17
Agnz2	D1Mit15-D1Mit155
Adaz1	D4Mit175-D4Mit187
Adaz2	D17Mit130

Table 3: Gene Knockout and Transgenic Murine Models with Lupus Manifestations

Knockout Model Genes	Transgenic Model Genes
Lyn	*Bcl-2*
CD22	*IFN-gamma*
SHP-1 (*me,* spontaneous)	*IL-4*
CTLA-4	*CD19*
Zfp-36	*Fli-1*
TGF-beta 1	
IL-2	
IL-2R-alpha	
IL-2R-beta	
Fas (lpr)	
FasL (gld)	
C1q	

Gene Knockouts Effects on Murine Lupus Models

Gene	Effect
ICAM-1	Improved Survival, Reduced Kidney Disease
NOS2	Decreased Vasculitis and IgG Rheumatoid Factor
TCR-alpha	Partial Inhibition of Disease
TCR-gamma	Exacerbated Disease
TCR-gamma/alpha	No Antibodies or Immune Complex Kidney Disease
Perforin	Exacerbated Disease
*Jh (*no B cells*)*	No Vasculitis or Glomerulonephritis
MHC Class II	Reduced Antibodies Titer and Glomerulonephritis
CD4	Reduced Antibodies Titer and Glomerulonephritis
MHC Class I	Reduced Lymphadenopathy
CD8	Reduced Lymphadenopathy
CD40L	Reduced Antibodies Titer and Glomerulonephritis
Fyn	Reduced Antibodies and Glomerulonephritis
IFN-gamma	Reduced Antibodies and Glomerulonephritis
IFN-gamma R	Reduced Antibodies and Glomerulonephritis
IL-4	Reduced Antibodies, Glomerulonephritis, and Lymphadenopathy
Fc-gammaR1	Prolonged Survival, Reduced Glomerulonephritis
C4	Reduced Antibodies and Glomerulonephritis
CD21/CD35	Reduced Antibodies and Glomerulonephritis

Table 4: Renal Parenchymal Cells: Chemokine, Cytokine and Growth Factor Profiles

	Chemokines	Cytokines	Growth Factors
Tubular Cells	MCP-1 MIP-1 RANTES IL-8 Opn	TNF-alpha IL-6 IL-12	TGF-beta PDGF
Mesangial Cells	MCP-1 RANTES IL-8	TNF-alpha IL-1 IL-6	TGF-beta M-CSF PDGF
Glomerular Epithelial Cells			PDGF beta-FGF
Renal Fibroblasts	RANTES	IL-1 IL-6	TGF-beta PDGF CTGF

Table 5: Adhesion Molecules and Vasculitic Diseases

Immune Complex Disorders
- Systemic Lupus Erythematosus
- Rheumatoid Vasculitis
- Henoch-Schoenlein Purpura
- Mixed Cryoglobulinemia
- Leukocytoclastic Vasculitis
- Polyarteritis Nodosa

Anti-Neutrophil Cytoplasmic Antibody Disorders
- Churg-Strauss Syndrome
- Microscopic Polyangiitis
- Wegener's Granulomatosis

T-Cell Response and Granuloma Disorders
- Giant Cell Arteritis
- Takayasu's Arteritis
- Kawasaki Disease

Table 6: ADHESION MOLECULES IN INFLAMMATION

Selectins (chromosome 1q)
- P-Selectin (CD62P): Platelets, Endothelial Cells
  - Synthesized by Megakaryocytes & Endothelial Cells
  - Stored in Alpha-Granules (platelets) and
  - Weibel-Palade bodies (endothelial cells)
  - Rapidly Expressed (<10 minutes)
  - Agonists: Histamine, Thrombin
  - Ligands: PSGL-1, CD24, CD15
- L-Selectin (CD62L): Constitutively Expressed on Surfaces of All Leukocytes
  - Ligands: GLYCAM-1, CD34, MAdCAM-1, CD15
- E-Selectin (CD62E): Synthesized by Activated Endothelial Cells
  - IL-1, TNF-alpha & beta, LPS Induced Synthesis
  - De Novo Synthesis Required (4 to 6 hours)
  - Ligands: ESL-1, PSGL-1, CD15
- Selectins Composed of:
  - Amino-Terminal Calcium-Binding Lectin Domain
  - EGF-Like Domain
  - Complement Binding Protein-Like Domain
  - Transmembrane Domain
  - Carboxyl-Terminal Cytoplasmic Domain
- Selectin Functions
  - Mediate First Steps in Leukocyte Adhesion
    - Capture (P-Selectin & L-Selectin)
    - Tethering (P-Selectin & L-Selectin)
    - Endothelial Activation
    - Rolling (P-Selectin, L-Selectin & E-Selectin)
    - Attachment/Adhesion (loose, E-Selectin & Integrins)
  - Initial Leukocyte Recruitment
  - Rapid Bond Formation to Promote Adherence
  - Rapid Dissociation to Facilitate Rolling
  - Favorable Free Energy: Resist Shear Forces

Integrin Adhesion Molecules
- LFA-1 (CD11a/CD18):
  - Polymorphonuclear Cells, Lymphocytes, Macrophages
  - Ligands: ICAM-1, 2 & 3
  - Antigen Stimulated T-Cell Priming (TCR)
  - Adhesion and Emigration into Tissue
- MAC-1 (CD11b/CD18):
  - Polymorphonuclear Cells, Macrophages
  - Ligands: ICAM-1 & 2, Fc, iC3b, Factor X, Fibrinogen
  - Expressed in Phagocytosis (iC3b)
  - Transmigration through Interstitial Tissue
- VLA-4 (CD49d/CD29):

Granulocytes, Lymphocytes, Macrophages
Ligand: VCAM-1, Fibronectin
Emigration into Tissue

Adhesion Molecules: Immunoglobulin Superfamily
ICAM-1 (CD54): Endothelial Cells (activated)
Ligands: CD11a/CD18 (LFA-1), CD11b/CD18 (Mac-1)
ICAM-2 (CD102): Endothelial Cells (activated)
Ligands: CD11a/CD18 (LFA-1), CD11b/CD18 (Mac-1)
VCAM-1 (CD106): Endothelial Cells (activated)
Ligand: CD49d/CD29 (VLA-4)
PECAM-1 (CD31): Endothelial Cells (activated),
Polymorphonuclear Cells, Macrophages
Ligand: PECAM-1

Leukocyte Recruitment, Adhesion and Emigration Into Tissue
Activated Leukocyte (Intravascular)
PSGL-1
E-Selectin Ligand
L-Selectin Ligand
Mac-1
LFA-1
Fc-gamma Receptor
Rolling: Initial Stage of Leukocyte Adhesion in Vessel
Selectins (P, E, L)
VLA-4
Firm Adhesion to Endothelium/Vessel Wall
LFA-1
Mac-1
ICAM-1
ICAM-2
VCAM-1
Leukocyte Extravasation/ Emigration into Tissue
LFA-1
Mac-1
ICAM-1
ICAM-2
VCAM-1
PECAM-1

Table 7: Adhesion Molecule Expression in Glomerulonephritis

Selectins

P-Selectin: Endothelial Surfaces of Glomerulus and Peritubular Epithelial Cells

E-Selectin: Endothelial Surfaces of Glomerulus and Interstitial Venules

Selectin Ligands CD34 (mucin): Constitutively Expressed by Glomerular Endothelial Cells

Integrins

ICAM-1: Endothelial Cells of Glomerulus, Peritubular Capillaries, Large Venules, Mesangium, Parietal Bowman's Capsule, Proximal Tubules, Fibroblast-like Interstitial Cells

VCAM-1: Parietal Bowman's Capsule, Large Venules, Peritubular Capillaries, Endothelial Cells of Glomerulus, Proximal Tubules

ICAM-2: Renal Endothelium

PECAM-1: Renal Endothelium

Table 8: Adhesion Molecule Targets in Renal Disease

Strategy for Inhibition of Leukocyte Adhesion in Animal Models
- Monoclonal Antibodies Against Adhesion Epitopes
- Soluble Adhesion Molecule Fragments or Analogs (Decoys)
- Anti-sense Oligonucleotides to Inhibit Adhesion Molecule Synthesis
- Regulate Endogenous Anti-Inflammatory Networks

Renal Diseases Affected by Inhibition of Adhesion Molecule Synthesis in Animal Models
- Acute Immune Complex Glomerulonephritis
- Crescentic Glomerulonephritis
- Hereditary Tubulointerstitial Nephritis
- Systemic Lupus Erythematosus-like GN
- Allograft Rejection
- Ischemic Acute Renal Failure

Table 9: Effect of ICAM-1 Knockout on FAS (lpr) Murine Lupus Model

	Fas	Fas/ICAM-1
Survival	26 weeks	47 weeks
BUN	62 mg/dL	21 mg/dL
IgG	10.4 mg/dL	8.0 mg/dL
Anti-DNA (double-stranded)	0.36 mg/dL	0.17 mg/dL

Effect of LFA-1 and Mac-1 Knockout on FAS (lpr) Murine Lupus Model

	LFA-1/Fas	Mac-1/Fas	Fas
Survival	41 weeks	22 weeks	24 weeks
BUN	24.8 mg/dL	43.8 mg/dL	38.1 mg/dL
Austin Lesion Score	4.9	11.9	16.8

Table 10: Current and Novel Therapies in Glomerulonephritis

Current Therapeutic Agents
- Glucocorticoids
- Cyclophosphamide
- Azathioprine
- Chlorambucil
- Mycophenolate mofetil
- Cyclosporine
- Tacrolimus
- Rapamycin
- 15-deoxyspergualin
- Leflunomide/FK778
- FTY720
- Plasma Exchange
- Intravenous Immunoglobulin
- Stem Cell Transplant

Immune/Inflammatory Component	Therapeutic Agent
Immune Response	
Antigen	LJP 394 (abetimus)
B Lymphocytes	Anti-CD20 (rituximab)
Costimulation	
CD40-CD154	Anti-CD154 (ICED-131, BG9588)
CD28-CD80-CD86	CTLA4 (CLTLA4-Ig, LEA29Y)
	Anti-CD80 (h1F1)
	Anti-CD86 (h3D1)
Antibody	Anti-idiotype (3E10)
Immune Complexes	DNAse
Immune Effectors	
Complement	Anti-CD5 (eculizumab)
Cytokines/Chemokines	
PDGF	STI571 (gleevec, imatinab)
TNF-alpha	Anti-TNF (infliximab)
	TNFR2-Ig (Rtanercept)
IL-1	IL-1ra (snakinra)
IL-10	Anti-IL10, rIL-10
MCP	Bindarit
Adhesion Molecules	
Beta1 Integrins	Anti-alpha4 integrin (natalizumab)
Beta2 Integrins	Anti-CD11a (efalizumab)
	Anti-CD18
ICAM-1	Anti-ICAM-1 (enlimomag)
	ICAM-1 Antisense Oligodeoxynucleotide (ISIS 2302, alicaforsen)
Cell Cycle	All trans-retinoic acid

	R-roscovitine (CY C202)
Fibrosis/Epithelial Mesenchymal Transition	Hepatocyte Growth Factor Bone Morphogenic Protein-7 Mutant Plasminogen Activator Inhibitor-1
Other Novel Therapies	
Bone Marrow Transplantation	
Nucleoside Analogs	Fludarabine, 2-Chlorodeoxyadenosine (2-CdA), Mycophenolate Mofetil Mizoribine, Leflunomide
T Cell-Directed Agents	MAX.16H5 (anti-CD4), CD5 Plus (anti-CD5 ricin A-chain immunoconjugate)
Anti-Idiotype & Competitive Peptides	
Anti-Inflammatory Drugs	Thromboxane Receptor Antagonist (DP-1904)

Potential Lupus Nephritis Therapy: Targeting B Cells

Agent	Mechanisms
Anti-CD20	Inhibit B-cell activation, proliferation and differentiation
Anti-CD40L	Block CD40/CD40L Interaction
CTLA4/Ig	Block B7/CD28 Interaction
CTLA4/Ig & Anti-CD40L	Co-block T and B Cell interactions
Anti-BLys	Inhibit B cell proliferation and differentiation
LJP-394	Tolerance Induction of anti-dsDNA producing B cells Reduce Anti-dsDNA Antibody
Anti-IL10	Block Effect of B Cell Mediator
Anti-IFN gamma	Inhibit B Cells, Reduce Autoantibody Production
Anti-C5b mAb	Block Complement Complex Attack
Anti-C3 (Cryy-Ig)	C3 Activity Regulation

References:

Bagavant H, Deshmukh US, Gaskin F, Fu M: Lupus glomerulonephritis revisited 2004: autoimmunity and end-organ damage. Scand J Immunol 60:52-63.

Bullard DC: Adhesion molecules in inflammatory disease: insights from knockout mice. Immunol Res 2002;26/1-3:27-33.

Bullard DC, King PD, Hicks MJ, Dupont B, Beaudet AL, Elkon KB: Intercellular adhesion molecule-1 deficiency protects MRL/MpJ-Fas-lpr mice from early lethality. J Immunol 1997;159:2058-67.

Ding ZM, Babensee JE, Simon SI, Lu H, Perrard JL, Bullard DC, Dai XY, Bromley SK, Dustin ML, Entman ML, Smith CW, Ballantyne CM: Relative contribution of LFA-1 and Mac-1 to neutrophil adhesion and migration. J Immunol 1999;163:5029-38.

Doyle HA, Yan J, Liang B, Mamula MJ: Lupus autoantigens: their origins, forms, and presentation. Immunol Res 2001:24/2:131-47.

Foster MH: Relevance of systemic lupus erythematosus nephritis animal models to human disease. Semin Nephrol 1999;19:12-24.

Graham DSC, Vyse TJ: The candidate gene approach: have murine models informed the study of human SLE? Clin Exp Immunol 2004;137:1-7.

Kelley VR, Wuthrich RP: Cytokines in the pathogenesis of systemic lupus erythematosus. Semin Nephrol 1999;19:57-66.

Kevil CG, Bullard DC: Roles of leukocyte/endothelial cell adhesion molecules in the pathogenesis of vasculitis. Am J Med 1999;106:677-87.

Kevil CG, Hicks MJ, He X, Zhang J, Ballantyne CM, Raman C, Schoeb TR, Bullard DC: Loss of LFA-1, but not Mac-1, protects MRL/MpJ-Fas-lpr mice from autoimmunity disease. Am J Pathol 2004;165:609-16.

Illei GG, Klippel JH: Novel approaches in the treatment of lupus nephritis. Lupus 1998;7:644-8.

Javaid B, Quigg RJ: Treatment of glomerulonephritis: will we ever have options other than steroids and cytotoxics? Kidney Int 2005;67:1692-703.

Su, W, Madalo MP: Recent advances in the pathogenesis of lupus nephritis: autoantibodies and B cells. Semin Nephrol 2003;23:564-8.

Tam FWK: Role of selectins in glomerulonephritis. Clin Exp Immunol 2002;129:1-3.

Theofilopoulos AN: Effector and predisposing genes in murine lupus. Lupus 1998;7:575-84

Tsao BP: Genetic susceptibility to lupus nephritis. Lupus 1998;7:585-90.

Tumlin JA: Lupus nephritis: novel immunosuppressive modalities and future directions. Semin Nephrol 1999;19:67-76.

CRYO-ELECTRON MICROSCOPY OF BIOLOGICAL TISSUE, CELLS AND ORGANELLES

J. M. Costello, PhD
Department of Cell and Developmental Biology
The University of North Carolina, Chapel Hill, N.C.

Cryo-electron microscopy is a rapidly expanding field that can be divided into two main areas: cryo-preservation for labeling or structural analysis and examination of specimens at low temperatures using a cryo-stage in a transmission electron microscope (TEM). Many types of specimens can be prepared using rapid cooling as the initial fixation step and the specimens can be examined, after processing, at ambient temperature or, without processing, directly at low temperature. Other samples, such as 2D crystalline arrays, can be stabilized with cryoprotectants and slowly cooled for examination at low temperature in a TEM. The choice of which cryo procedure to use is often dictated by the dimensions of the sample. This brief review summarizes the procedures and types of equipment currently available to examine a size range from large samples, such as portions of tissues and organs, to small samples, such as virus particles or cellular components.

The main goals of cryo-preservation with ultrarapid freezing are to stabilize the biological material in its natural state and avoid ice crystal formation and damage. Ultrarapid freezing procedures can be classified based on the physical technique used to extract heat from a specimen. Plunge freezing is the oldest and most commonly used, in part, because of the simplicity of dropping a sample into liquid coolant. The success of plunge freezing, as with other methods, is often based on scale: mm sized tissue fragments in the absence of cryoprotectants cannot usually be frozen without ice crystal damage, some cells in the 20-100 μm range can occasionally be well-preserved, and fragments of cells, including organelles or molecular complexes, can often be perfectly preserved within a matrix of amorphous or vitreous ice. The critical parameter is the thickness of the sample, which should be less than 10 μm. Thus, small cells or fragments sandwiched between thin copper disks can be well preserved by plunging into liquid propane. These frozen samples will probably contain microcrystalline ice that causes little or no damage. To obtain truly amorphous or vitreous ice, the samples must be even thinner, about 100 nm or less. Cell components, single particles and model systems, which can be prepared in a thin aqueous layer suspended over a holes in a support film on an electron microscope grid, can be vitrified by plunging into liquid ethane (a slightly better coolant than propane). This has become the preferred method to consistently prepare biological samples embedded in amorphous ice (the so called, “frozen hydrated” samples) for direct examination in the TEM using a cryotransfer system (to avoid ice crystal deposition on the cold sample) and a cold stage to maintain a stable temperature in the range of -140°C to –170°C (1). Several commercial devices have optimized each critical step in the freezing process, such as blotting the grid to produce a uniformly thin layer (2). These new devices permit a relatively inexperienced user to obtain reproducibly excellent sample preservation in amorphous ice.

An alternative to plunge freezing is to spray a stationary, sandwiched sample with jets of propane from opposite sides. This “propane jet” method gives slightly higher cooling rates compared to the same sample plunged into coolant and thus gives somewhat better preservation of samples 10-20 μm thick (3). A distinct method of bringing sample and coolant into contact forces the flat surface of a sample onto a stationary, liquid-helium-cooled copper block. This is the “quick

freeze" or "slam cooling" method that is often followed by deep etch, rotary shadowing with platinum/carbon (4). The advantage is that cooling is rapid enough to vitrify the surface of the sample without mechanical damage. The limitations are that only a 10 μm thick layer is consistently well preserved and most samples have to be pre-washed in a volatile buffer to allow deep etching. Many sample types have been shown to withstand these treatments and the subsequent images of cellular substructure of often unique and stunning. Large tissue fragments can be slam frozen, as long as a flat region containing the structures of interest can be exposed at the surface that will contact the copper block.

Many samples that do not need to be rapidly cryofixed can be treated with cryoprotectants prior to cooling. The most common cryoprotectants are small molecule solutes that complex water, such as glycerol, sucrose and trehalose (a naturally occurring plant diglucose). When used for example at a concentration of 10-30%, ice crystal formation and growth are sufficiently retarded that relatively slow freezing can be used to give excellent structural preservation. These samples can be frozen by a variety of methods producing slow or modest cooling rates. The test of the extent of preservation is the condition or resolution of the frozen samples, which can be examined in many different ways. For example, thin 2D crystalline arrays of aquaporins embedded in glucose on electron microscope grids were analyzed by cryoelectron crystallography at high resolution (5). In separate procedures large cryoprotected tissue pieces can be cryosectioned, the sections warmed and immunogold labeled for localization analysis at room temperature (6). The cryosections can also be examined at low temperature in a cold stage without stains or artificial contrasting treatments (7).

A different approach to cryoprotection is employed in high pressure freezing (HPF) where the aqueous sample is exposed to a pressure of about 2000 bar just prior to freezing with a coolant, such as a jet of liquid nitrogen (8). The high pressure acts as a cryoptotectant by greatly lowering the temperature of ice crystal nucleation. The main advantage of HPF is that samples typically about 200 μm in the smallest dimension can be preserved throughout in amorphous ice. Such properly frozen macro samples have aqueous regions that are completely clear immediately after freezing. The subsequent processing of the HPF frozen sample generally follows one of three paths: cryosectioning, freeze fracture or freeze substitution. Recent advances in cryosectioning, using a diamond knife connected to an oscillator, have demonstrated that minimally distorted sections can be cut to a thickness of 50 nm and that, when examined using a TEM cold stage, the electron diffraction pattern shows that the ice is amorphous throughout the section (9). This offers the opportunity to study tissues in their natural state and to perform high-resolution cryotomography using only the natural contrast (10). These approaches are still being refined and hold great promise because of the wide applicability to a variety of large structures that loose their biological integrity when dissected or manipulated to conform to other preparation techniques.

After HPF, samples can be freeze fractured conventionally or deep etch, rotary shadowed. In this case the region of interest is exposed at the fracture interface, which is in part dependent on the method of loading the sample into the HPF holder. Access to the entire interior of the HPF frozen sample is available after freeze substitution. Two general approaches to freeze substitution are preservation for structural or labeling analysis. Structural analysis commonly uses osmium tetroxide in anhydrous acetone as the substitution medium for several days at about -90°C. Water molecules are slowly replaced by organic solvent molecules, while the biological structure is immobilized at low temperature. During slow warming, the osmium tetroxide

contributes to the fixation of lipids and proteins, as well as produces stain contrast. After warming, the samples are processed as in conventional TEM including final embedding in an epoxy resin. Additional contrast is obtained by staining thin sections with tannic acid and heavy metals. The second approach commonly employs a non-osmium medium containing mild fixatives, such as uranyl acetate or a small amount of glutaraldehyde. Water soluble resins, such as Lowicryl or LR White for embedding after warming, seem to preserve antigenicity for subsequent labeling of thin sections at room temperature.

In summary, cryo-preservation can be accomplished using a variety of methods appropriate for the specific tissue geometry and the desired structural information. For the highest resolution, thin frozen hydrated samples examined at low temperature are desirable, and special high voltage TEMs are often required to reach the maximum resolution. For cells in culture or naturally thin samples, some form of sandwich holder may be suitable for many applications. For a variety of sample sizes and shapes, HPF offers many advantages as long as the final output is appropriate. If the primary scientific issue is the visualization of the cytoskeleton or extracelluar matrix fibers, perhaps only deep etch, rotary shadowing following slam freezing will be suitable. Today there are many options available to find the appropriate sample cryo-EM preparation procedure suitable for most morphological projects.

References.

1. Dubochet, J., Adrian, M., Chang, J. Homo, J., Lepault, J., McDowall, A., and Schultz, P. Cryo-electron microscopy of vitrified specimens. Quar. Rev. Biophys. 21, 129-228, 1988.
2. Frederik, P. Cryo-electron microscopy to follow macromolecular interactions on the grid and on the grid processing. Microsc. Microanal. 10 (Suppl 2), 424-425, 2004.
3. Muller, M., Meister, N. and Moor, H. Freezing in a propane jet and its application in freeze-fracturing. Mikroskopie 36, 129-140, 1980.
4. Hirokawa, N. and Heuser, J. Quick-freeze, deep-etch visualization of the cytoskeleton beneath surface differentiations of intestinal epithelial cells. J. Cell Biol. 91, 399-409, 1981.
5. Schenk, A. et al., The 4.5A structure of human AQP2. J. Mol. Biol. 350, 278-289, 2005.
6. Gleeson, P., Anderson, T., Stow, J., Griffiths, G., Toh, B. and Matheson, F. p230 is associated with vesicles budding from the trans-Golgi network. J. Cell Sci. 109, 2811-2821, 1996.
7. Al-Amoudi, A., et al. Cryo-electron microscopy of vitreous sections. EMBO J. 23, 3583-8, 2004.
8. Studer, D., Graber, W., Al-Amoudi, A and Eggli, P. A new approach for cryofixation by high-pressure freezing. J. Microsc. 203, 285-294, 2001.
9. Al-Amoudi, A., Dubochet, J., Gnaegi, H. Luthi, W. and Studer, D. An oscillating cryo-knife reduces cutting-induced deformation of vitreous ultrathin sections. J. Microsc. 212, 26-33, 2003.
10. McIntosh, R., Nicastro, D. and Mastronarde, D. New views of cells in 3D: an introduction to electron tomography. Trends in Cell Biol. 15, 43-51, 2005.

THREE-DIMENSIONAL STRUCTURE OF THE GLOMERULAR SLIT DIAPHRAGM AS REVEALED BY ELECTRON TOMOGRAPHY

Karl Tryggvason, MD, PhD
Division of Matrix Biology
Department of Medical Biochemistry and Biophysics
Karolinska Institute, Stockholm, Sweden

The renal glomerular filter constitutes three layers: a fenestrated endothelium, glomerular basement membrane (GBM), and the slit diaphragm located between the interdigitating foot processes of the podocytes that cover the capillary surface. While the unique morphology of the glomerular filtration barrier has been well known for decades, the molecular nature of the filtration barrier, thought to be a size- and charge-selective filter, has been poorly understood. However, in recent years, the significant role of the slit diaphragm has become increasingly appreciated (1, 2).

The slit diaphragm has for long been observed in electron microscopy as a fine line between the podocyte foot processes. In the 1970s Rodewald and Karnovsky (3) proposed, based on their electron microscopic findings, that the slit diaphragm is an about 40 nm wide, isoporous zipper-like structure where staggered cross-bridges extend from adjacent podocytes to a longitudinal central filament and form rectangular pores in the slit diaphragm. This model was questioned following results with freeze-etching replicas of unfixed rat kidney, which suggested a sheet-like, rather than a zipper-like substructure (4). The molecular nature of this vital ultrafilter remained obscure until in the late 1990s.

Through positional cloning of the gene mutated in congenital nephrotic syndrome of the Finnish type (CNF), nephrin, a unique component of the slit diaphragm was identified (5). Nephrin that is specifically located in podocyte foot processes (6), is a transmembrane protein with a short intracellular domain short intracellular domain rich in serine and tyrosine residues, a transmembrane domain and an extracellular domain containing eight distal IgG-like motifs and a proximal fibronectin type III repeat. Based on the primary structure, it could be predicted that each nephrin molecule is about 30 nm long and it was hypothesized that nephrin molecules from adjacent foot processes interact in the center of the slit to form a zipper like formation (7). This model would allow for holes on each side of a central density, essentially as predicted by Karnovsky. Support for such a structure came from studies showing homologous interactions of nephrin molecules in solution and in transfected cells, interactions that could be disrupted with antibodies directed against the extracellular domain. Three novel membrane proteins, Neph1, Neph2 and a large protocadherin FAT1 have also been localized to the slit diaphragm proper and shown to be essential for its function (see (1, 2, 8). In addition to those, several intracellular proteins such as, podocin, CD2AP, ZO-1 have been shown to be an important part of a slit diaphragm protein complex (for review, see (1, 2)). Ablation of the genes for most of those proteins causes proteinuria, demonstrating the importance of the proteins for filtration.

In order to elucidate the three dimensional-structure of the slit diaphragm, we have used a novel electron tomography (ET) technique. ET has opened up for new possibilities for molecular analysis of cellular constituents (9, 10). It is the only 3D reconstruction method not based on averaging. Therefore, it makes imaging (11, 12) and immunoidentification (13, 14) of individual macromolecular structures possible in their cellular context, usually at some 5 to 10-nm resolution. Combined with high-resolution structural approaches (e.g. X-ray crystallography, nuclear magnetic resonance, and single-particle analysis by cryo-electron microscopy), ET also provides the possibility to perform multi-resolution docking of structural details of component molecules into macromolecular complexes in cellular organelles and substructures (15).This has opened up wider prospects for mapping territorial distribution of macromolecules and analysis of molecular interactions *in situ*, both in sections and in intact frozen cells.

In our analysis of thin resin and cryo-sections of fixed human, rat, and mouse kidneys, the SD was shown to be as a porous network of molecular strands with globular substructure (16). The results were confirmed in fixed and unfixed mouse kidneys using high-pressure-freezing and freeze-substitution. Immunoelectron microscopy and immuno-ET revealed the presence and orientation of nephrin molecules in the SD network. Glomeruli from CNF patients and nephrin knockout mice lacked the SD network and its group of characteristic strands, and the slit had collapsed to only about 10-15 nm in width. Analysis of individual nephrin molecules in transfected cells and in solution showed that nephrin molecules, identified by anti-nephrin antibodies, appear as convoluted strands similar to those observed in the normal slit diaphragm *in situ*. Based on these findings, we propose a nephrin-containing network-model for the structure of the slit diaphragm. It takes into consideration the EM localization of nephrin, the structural characteristics of the molecule, and the novel ET findings. The present findings result in a partly molecular-level version of the Rodewald and Karnovsky zipper-model (3) where nephrin strands from the two opposing slit sides cross the slit diaphragm and form filtration channels, too small for albumin-sized molecules to pass. Molecular interactions may exist between the nephrin strands, most notably at the slit center. Other molecular types, at present not identified on the ET level, may well contribute to the network. The model also allows for a proposed dynamic nature of the slit diaphragm Changes in the slit diaphragm width could take place by stretching of the coiled and bent cross-strands and explain, in part, the variations seen by different methods in slit diaphragm length and appearance.

References

1. Somlo S, Mundel P. Getting a foothold in nephrotic syndrome. Nat Genet 2000;24(4):333-5.
2. Tryggvason K, Wartiovaara J. How does the kidney filter plasma? Physiology (Bethesda) 2005;20:96-101.
3. Rodewald R, Karnovsky MJ. Porous substructure of the glomerular slit diaphragm in the rat and mouse. J Cell Biol 1974;60(2):423-33.
4. Hora K, Ohno S, Oguchi H, Furukawa T, Furuta S. Three-dimensional study of glomerular slit diaphragm by the quick-freezing and deep-etching replica method. Eur J Cell Biol 1990;53(2):402-6.
5. Kestila M, Lenkkeri U, Mannikko M, et al. Positionally cloned gene for a novel glomerular protein--nephrin--is mutated in congenital nephrotic syndrome. Mol Cell 1998;1(4):575-82.
6. Ruotsalainen V, Ljungberg P, Wartiovaara J, et al. Nephrin is specifically located at the slit diaphragm of glomerular podocytes. Proc Natl Acad Sci U S A 1999;96(14):7962-7.
7. Tryggvason K. Unraveling the mechanisms of glomerular ultrafiltration: nephrin, a key component of the slit diaphragm. J Am Soc Nephrol 1999;10(11):2440-5.
8. Gerke P, Sellin L, Kretz O, et al. NEPH2 is located at the glomerular slit diaphragm, interacts with nephrin and is cleaved from podocytes by metalloproteinases. J Am Soc Nephrol 2005;16(6):1693-702.
9. McEwen BF, Marko M. The emergence of electron tomography as an important tool for investigating cellular ultrastructure. J Histochem Cytochem 2001;49(5):553-64.
10. Baumeister W. Electron tomography: towards visualizing the molecular organization of the cytoplasm. Curr Opin Struct Biol 2002;12(5):679-84.
11. Bohm J, Frangakis AS, Hegerl R, Nickell S, Typke D, Baumeister W. Toward detecting and identifying macromolecules in a cellular context: template matching applied to electron tomograms. Proc Natl Acad Sci U S A 2000;97(26):14245-50.
12. Medalia O, Weber I, Frangakis AS, Nicastro D, Gerisch G, Baumeister W. Macromolecular architecture in eukaryotic cells visualized by cryoelectron tomography. Science 2002;298(5596):1209-13.
13. Wetterberg I, Zhao J, Masich S, Wieslander L, Skoglund U. In situ transcription and splicing in the Balbiani ring 3 gene. Embo J 2001;20(10):2564-74.
14. Ziese U, Kubel C, Verkleij A, Koster AJ. Three-dimensional localization of ultrasmall immuno-gold labels by HAADF-STEM tomography. J Struct Biol 2002;138(1-2):58-62.
15. Sandin S, Ofverstedt LG, Wikstrom AC, Wrange O, Skoglund U. Structure and flexibility of individual immunoglobulin G molecules in solution. Structure (Camb) 2004;12(3):409-15.
16. Wartiovaara J, Ofverstedt LG, Khoshnoodi J, et al. Nephrin strands contribute to a porous slit diaphragm scaffold as revealed by electron tomography. J Clin Invest 2004;114(10):1475-83.